Fachtagung "Lasermethoden in der Strömungsmesstechnik"
3. – 5. September 2013, München

Erzeugung von Geschwindigkeitsverteilungen aus Single Pixel Correlation PIV

Reconstruction of velocity distributions from single pixel correlation PIV

Michael Manhart, Claudia Strobl
Technische Universität München, Fachgebiet Hydromechanik, Arcisstr. 21, 80333 München

PIV, turbulente Strömungen, Verteilungsfunktion der Geschwindigkeiten
Particle Image Velocimetry, turbulent flows, velocity probability density

Abstract

The ensemble correlation method for particle image velocimetry (PIV) is shown to contain the joint velocity probability density function. The velocity probability density function (PDF) can be interpreted as a deterministic part in the ensemble correlation of PIV images. The correlation with particle images at other locations can be interpreted as a random part. The probability of the random part can be quantified in terms of the auto-correlation of the intensity of the first image and the probability density of the velocity. Thereby, it can be eliminated from the correlation functions to obtain the velocity PDF. Thus, the velocity PDF can be obtained at single pixel resolution in both, laminar and turbulent flows. The accuracy of the method is assessed by using synthetic PIV images in terms of various parameters such as particle density, number of image pairs, and pixel resolution of the velocity distribution.

1. Introduction

Particle Image Velocimetry (PIV) is one of the state-of-the-art non-intrusive measurement techniques for laminar and turbulent flows. It allows for instantaneous measurement of 2D or even 3D velocity fields. For turbulent flows, in most cases statistical moments of the joint velocity distribution function are computed, like the average flow or elements of the Reynolds stress tensor or higher moments. The standard algorithm for PIV (that is also available in commercial PIV systems) uses interrogation windows to compute the correlation of two consecutive images of particles in the flow field. The correlation peak marks the mean displacement of the particles inside of the interrogation window. Thus it determines instantaneous velocity vectors that are spatially averaged over one interrogation window. The interrogation window technique has therefore the disadvantage of a loss of spatial resolution as in most cases 16 or 32 pixels have to be used for one interrogation window to obtain a sufficient number of particles for a well pronounced correlation peak. This is especially problematic in situations in which a strong mean shear is present in the velocity field, which smears the correlation peak. For such situations techniques have been developed that use sheared images (Raffel et al. 2007).
Meinhard & Werely 2000 proposed to use more than one image pair to compute the image correlation (ensemble correlation technique). Thus, the signal-to-noise ratio can be improved without using larger interrogation windows. The spatial resolution is improved at the cost of temporal resolution. Westerweel et al. 2004 used this method for the evaluation of micro-

scopic PIV data to improve the spatial resolution. They emphasize the fact that in laminar flows a single pixel resolution can be obtained. They determine the (laminar) velocity vector from the peak of the single pixel correlation of the image pairs. The number of samples required for a pronounced correlation peak is obtained by increasing the number of window pairs. The authors state however that only in steady flow situations a clear correlation peak can be achieved as the peak is smeared out in turbulent flows. Subsequently, the single pixel ensemble correlation technique has been used successfully by several authors in the field of micro-PIV in which laminar flows are present.
Kähler et al. 2006 assess the ensemble correlation technique as proposed by Westerweel et al. 2004 in a turbulent boundary layer flow. They are able to measure time averaged velocities at high accuracy and conclude that it is a useful technique for assessing averaged flow vectors at high spatial resolutions. This is especially useful close to the wall where the use of an interrogation window would limit the resolution. The ensemble correlation technique can improve the spatial resolution considerably. However, a direct measurement of the Reynolds stresses was not possible with these first approaches.
The single pixel correlation function contains the joint velocity probability function (jPDF) as pointed out by Scharnowski et. al. 2012. In principle, if that function was known, all moments of the jPDF could be determined including the Reynolds stress tensor, skewness and flatness. The problem is the low signal-to-noise ratio that inhibits a direct determination of the moments. Scharnowski et. al. 2012 proposed to fit a 2D multivariate Gaussian into the correlation peak. They demonstrate that for certain kinds of flows, the Reynolds stress tensor can be estimated up to a reasonable accuracy. However, this approach is limited to Gaussian velocity distributions and therefore might not be applicable in wall proximity as the velocity signals there strongly deviate from Gaussian behavior (Moser et al. 1999).
In this manuscript, we emphasize that the correlation between two PIV images contains two parts, a deterministic displacement of the intensity of the first image due to the flow vector and a random part due to the random correlation of different particles. We quantify both contributions in terms of the auto-correlation of the intensity of the first image and the probability density of the velocity. By this we are able to subtract the random part and to directly determine the jPDF of the velocity from particle image pairs to single pixel accuracy.
The manuscript is organized as follows. The next section introduces the theoretical background used in the technique. Section 3 describes a method to demonstrate the proof of concept of the technique by synthetic images. A consistent parameter study is used in section 4 to determine the dependence of the accuracy of the method on parameters such as number of image pairs and type of induced velocity PDF.

2. Theory

We demonstrate that the correlation function of two images of randomly distributed particles displaced by a certain velocity vector within a time interval Δt contains two contributions, a deterministic and a random one. We start by defining the intensity of each image. The intensity of the first image is denoted by $I_1(\boldsymbol{x})$, the one of the second image by $I_2(\boldsymbol{x})$. The intensity of the first image is given by a random distribution of particles in space $W_1(\boldsymbol{x})$ convolved by the intensity function of a single particle I_S. So, $I_1(\boldsymbol{x})$ can be written as

$$I_1(\boldsymbol{x}) = \int W_1(\boldsymbol{x}-\boldsymbol{s}) I_S(\boldsymbol{s}) d\boldsymbol{s} \tag{1}$$

As the position of the particles in the second image result from the displacement $\boldsymbol{r}$ of the particles in the first image due to the local velocity vector $\boldsymbol{v}(\boldsymbol{x}) = \boldsymbol{r}/\Delta\mathrm{t}$ within the time interval Δt

of the two consecutive images, the particle distribution of the second image can be described by the following expression:

$$W_2(\boldsymbol{x_2}) = W_1(\boldsymbol{x_1})\delta(\boldsymbol{x_2} - (\boldsymbol{x_1} + \boldsymbol{r})) \tag{2}$$

with δ being the Kronecker delta used as sifting function. As $\boldsymbol{v}(\boldsymbol{x})$ and $\boldsymbol{r}$ are functions of space, the intensity of the second image is obtained as

$$I_2(\boldsymbol{x_2}) = \int W_2(\boldsymbol{x_2} - \boldsymbol{s})I_S d\boldsymbol{s} = \int W_1(\boldsymbol{x_1} - \boldsymbol{s})\delta(\boldsymbol{x_2} - (\boldsymbol{x_1} + \boldsymbol{r}))\, I_S(\boldsymbol{s})d\boldsymbol{s} \tag{3}$$

In other words the intensity of the second image can be expressed by intensity of the first image shifted by the displacement vector. So the intensity of the second image contains two contributions which result from a shift of the intensity from $\boldsymbol{x}_1$ to $\boldsymbol{x}_2 = \boldsymbol{x}_1 + \boldsymbol{r}$ (deterministic) and from the other points to $\boldsymbol{x}_2 \neq \boldsymbol{x}_1 + \boldsymbol{r}$. The latter contribution is not correlated to the intensity at $\boldsymbol{x}_1$ due to the random nature of the particle distribution in the first image. It can be regarded as random part contributing to the noise in the correlation function.

The single pixel correlation technique is based on the correlation of single pixels of image pairs:

$$R(\boldsymbol{x}_1, \boldsymbol{x}_2) = \langle I_1(\boldsymbol{x}_1) I_2(\boldsymbol{x}_2) \rangle \tag{4}$$

Using the fact that the second image can be decomposed in a deterministic and a random part, the correlation function $R(\boldsymbol{x}_1, \boldsymbol{x}_2)$ can as well be written as the sum of a deterministic and a random part.

$$R(\boldsymbol{x}_1, \boldsymbol{x}_2) = R^{det} + R^{rand} = \langle I_1^2(\boldsymbol{x}_1) \rangle P\left(\boldsymbol{v} = \frac{\boldsymbol{r}}{\Delta t}\right) + \langle I_1(\boldsymbol{x}_1) \rangle \langle I_2(\boldsymbol{x}_2) \rangle \left(P\left(\boldsymbol{v} \neq \frac{\boldsymbol{r}}{\Delta t}\right)\right) \tag{5}$$

Taking into account that the probability of the random contribution $P(\boldsymbol{v} \neq \boldsymbol{r}/\Delta t)$ can be expressed by $1 - P(\boldsymbol{v} = \boldsymbol{r}/\Delta t)$, with $P(\boldsymbol{v} = \boldsymbol{r}/\Delta t)$ being the probability of the deterministic part, it is possible to quantify the random part of the correlation function. Solving Eq. (5) for $P(\boldsymbol{v} = \boldsymbol{r}/\Delta t)$ gives the velocity probability density function (PDF):

$$P\left(\boldsymbol{v} = \frac{\boldsymbol{r}}{\Delta t}\right) = \frac{\langle I_1(\boldsymbol{x_1}) I_2(\boldsymbol{x_2}) \rangle - \langle I_1(\boldsymbol{x_1}) \rangle \langle I_2(\boldsymbol{x_2}) \rangle}{\langle I_1^2(\boldsymbol{x_1}) \rangle - \langle I_1(\boldsymbol{x_1}) \rangle \langle I_2(\boldsymbol{x_2}) \rangle} \tag{6}$$

3. Description of synthetic test images

We are using synthetic images to test our approach. Thereby we can impose a certain velocity PDF and compare whether our estimated PDF's converge to the imposed ones. Therefore synthetic images with different parameters were generated. The size of the images was set quite small compared to actual PIV images as we only reconstruct the velocity PDF at the central point of the images. The range of pixels/bins was varied from 20 to 61 in one direction.

The first image of an image pair was created by generating a random distribution of particles, each covering exactly one pixel. In this step of the study, we used a particle size of one pixel. The particle density was varied between 1 and 50 percent. The second image of an image pair was generated by a displacement of the first image by a certain displacement vector corresponding to a velocity vector. The velocity or displacement vector, respectively, was generated by a random number generator giving either a Gaussian or a positive/negative skewed normal distribution.

Thus a large number of image pairs, each representing a certain velocity, was generated and in total all of these image pairs contribute to the desired velocity PDF. By variation of the number of image pairs the dependence of the accuracy of the algorithm on the number of image pairs could be determined.
To evaluate the algorithm we computed the image correlation from which the velocity PDF has been determined using Eq. (6). This PDF is being compared with the imposed one. The same we do for the first and second moment of the PDF, the mean and the root mean square of the fluctuations.
To assess the level of accuracy of the proposed method certain parameters were varied, such as the number of pixels representing the induced PDF of the velocity as well as the number of images used and the number of pixels/bins of the images themselves. In this contribution we demonstrate the basic capabilities of our approach in a 1D setting.

4. RESULTS AND DISCUSSION

As described in the previous section the new algorithm was tested for various parameter sets. For clarity we restrict ourselves in the following figures to a 1D situation showing displacements, correlation functions and velocity PDF's in x-direction only. This is useful to be able to assess the dependence of the results on various parameters of the algorithm. It has to be noted that an extension to two-dimensional situations is straightforward.

In Fig. 1 the fundamental relationship, Eq. (5), is demonstrated. The x-axis represents the displacement $\boldsymbol{x}_2$. The correlation function $\boldsymbol{R}(\boldsymbol{x}_1, \boldsymbol{x}_2)$ is plotted for a fixed position $(\boldsymbol{x}_1 = 0)$and all functions are normalized by $I_1^2(\boldsymbol{x}_1)$. It can be seen, that the correlation function does not decay at large displacements as it should and that it is somehow shifted upwards compared to the imposed PDF. This is due to the random part of the correlation. By applying the correction, Eq. (6), to the correlation, the PDF of the velocity, which is the deterministic part of the correlation function, can be reconstructed. One can see in Fig. 1 that this was successful. Note, that here 500.000 image pairs at a particle density of 5% were used. This gives a number of 25.000 velocity samples to obviously minimize the statistical error.

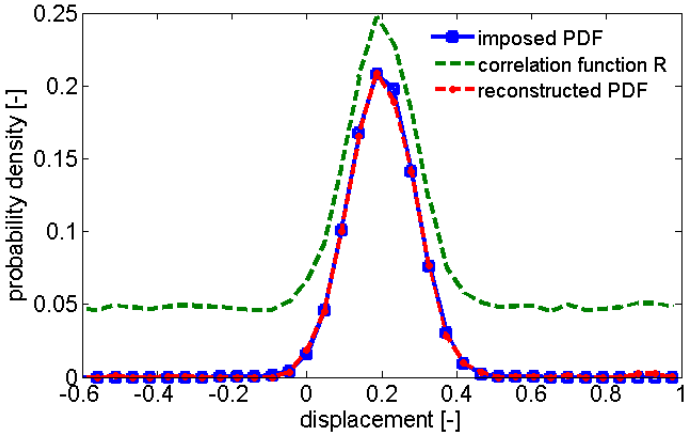

Fig. 1: Comparsion of imposed PDF, normalized result of single-pixel correlation R and reconstructed PDF, 43 bins, particle density 5 %, 500.000 images.

In a next step we investigate how the estimated PDF converges to the one which was imposed by the random number generator used for the displacement velocities. In Fig. 2 the velocity PDF's estimated from the single pixel correlation function at various numbers of image pairs have been plotted. For this investigation it is important to note that the imposed PDF's change with an increasing number of image pairs and converge to the one that is plot-

ted in Fig. 1. The reconstructed PDF's therefore can only reconstruct the PDF's at a given number of image pairs. The error in evaluating the velocity distribution consists here of two contributions: (i) the statistical error of the actual velocities and (ii) the error due to the correlation method. With increasing number of image pairs, both errors converge to zero.

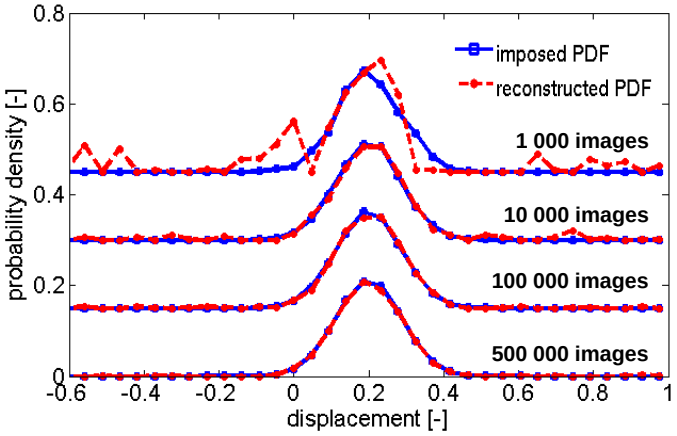

Fig. 2: Convergence of the reconstructed PDF towards imposed PDF with increasing number of images: 43 bins, particle density 5%. Plots for different numbers of image pairs are shifted for clarity.

As the derivation of Eq. (5) is independent of the form of the PDF, there is no need for it to be Gaussian. To examine how well non-Gaussian PDFs are estimated, we generated displacement velocities according to a skewed Normal distribution. In Fig. 3, we observe that the convergence, noted in Fig. 2 for a Gaussian shaped PDF, is also obtained for non-Gaussian PDFs. They are reproduced within a similar level of accuracy as the Gaussian ones.

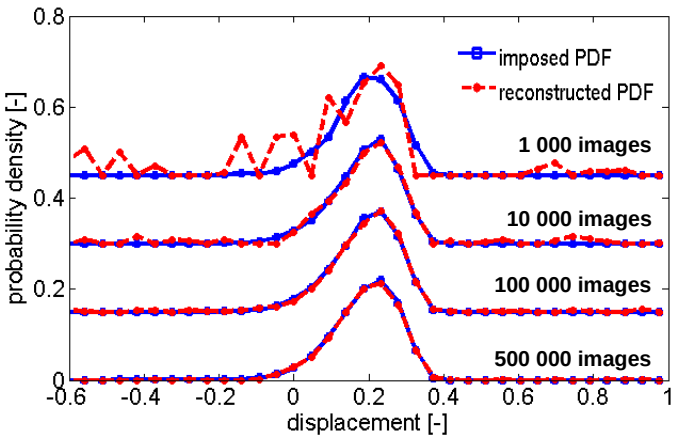

Fig. 3: Comparison of imposed PDF with reconstructed PDF for a skewed Normal distribution. 43 bins, particle density 5%. The plots for different numbers of image pairs are shifted for clarity.

Further on, we estimated the convergence of the first and second moment of the velocity PDF with the increasing number of image pairs. In Table 1, estimated mean velocities (first moment) as well as the second moments are compared to the imposed ones for Gaussian PDFs.

Tab. 1: Convergence of the 1st and 2nd moment of the reconstructed Gaussian distributed velocity PDF with increasing number of images, 43 bins, particle density 5%.

number of images	imposed <u>	reconstructed <u>	error in <u> [%]	imposed U_{rms}	reconstructed U_{rms}	error in U_{rms} [%]
1 000	0.2004	0.1765	11.91	0.0860	0.0932	-8.43
10 000	0.1999	0.2016	-0.87	0.0866	0.0961	-10.89
100 000	0.1999	0.2015	-0.78	0.0875	0.0922	-5.35
500 000	0.2000	0.1978	1.14	0.0877	0.0901	-2.79

In Table 2 a comparison of the first and second moment of the skewed Normal distribution is given. What has been already observable in Fig. 1 and 2 can also be seen here: with an increasing number of image pairs, the mean velocity as well as the root mean square will converge to the imposed values. One should note that due to the binary set up of the image (pixel covered by a particle contains value 1, empty pixel contains value 0) an effect similar to peak locking will occur, so that the error in the mean velocity will fluctuate in the range of 1%.

Tab. 2: Convergence of the 1st and 2nd moment of the reconstructed skewed normal distributed velocity PDF with increasing number of images, 43 bins, particle density 5%.

number of images	imposed <u>	reconstructed <u>	error in <u> [%]	imposed U_{rms}	reconstructed U_{rms}	error in U_{rms} [%]
1 000	0.1894	0.1644	13.22	0.0865	0.1193	-37.88
10 000	0.1885	0.1745	7.44	0.0877	0.1283	-46.32
100 000	0.1883	0.1856	1.40	0.0891	0.1003	-12.62
500 000	0.1882	0.1866	0.85	0.0892	0.0899	-0.74

Besides the influence of an increasing number of image pairs we tested the dependency on the number of pixels resolving the velocity PDF. In Fig. 4 the development of the error in the mean as well as of the root mean square of the velocity is shown when coarser representations of the PDF are used. The distributions shown so far used 19 pixels to cover the whole PDF. Coarser representations give larger error, however, the increase is not very high. With a rather rough resolution of the PDF of 7 pixels the error in the mean velocity is still lower than ten percent.

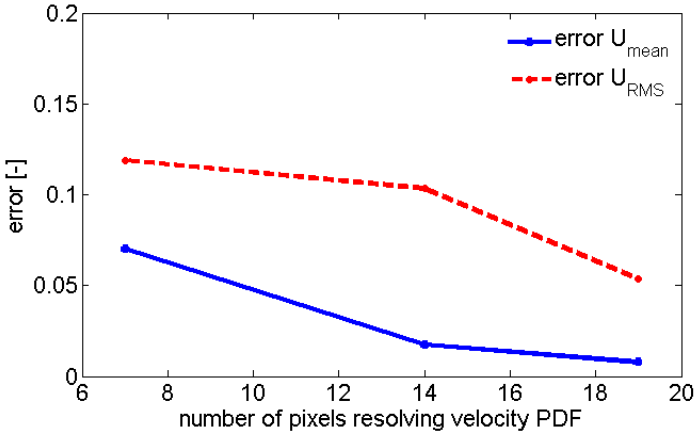

Fig. 4: Development of the errors in the 1st and 2nd moment of the reconstructed velocity PDF: 100 000 images, 5% particle density, Gaussian shaped imposed PDF

So far all tests were shown with only 5% of the pixels covered by particles. In Figure 5 the dependency of the errors in the mean and in the root mean square of the velocity on the particle density are shown. It can be seen that, as one would expect, with a rise of covered pixels also the error increases. The best results can be gained in the range of 1 to 10% of the image covered by particles. But in this case one should take into account that when creating the synthetic images always one pixel was set to a value of 1.0 when a particle position was within the area of the pixel. So if by accident two particle positions laid within one pixel then this second particle would not be accounted setting up the intensity distribution leading to an increase of error from overlapping particle images.

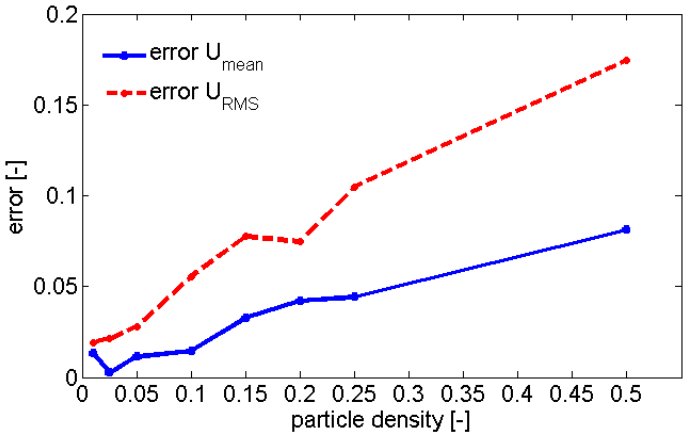

Fig. 5: Development of the errors in the 1st and 2nd moment of the reconstructed velocity PDF: 43 bins, 500 000 images, Gaussian shaped imposed PDF

5. CONCLUSION

We derived theoretically, that the correlation of two consecutive PIV images consists of two parts, a deterministic one stemming from the displacement of the particles by the fluid velocity and a random one stemming from the random placement of particles. Removing the random part gives us the opportunity to directly determine the PDF of the velocity from particle image pairs to single pixel accuracy.

Based on this observation, we propose an algorithm to reconstruct the velocity PDF directly from PIV image pairs. We tested the algorithm using synthetically generated PIV images with the advantage that the imposed velocity PDF was known exactly. Thus we were able to demonstrate that

- the reconstructed PDF converges to the imposed one with an increasing number of image pairs,
- the first and second moments of the reconstructed PDF converge to the imposed ones with increasing number of image pairs,
- non-Gaussian velocity PDF's are reconstructed as well as Gaussian PDF's

One has to note that so far we only demonstrated a proof of concept. The method is converging with number of image pairs. Two main advantages over conventional estimation of PIV image pairs with interrogation windows can be stated: first an accuracy of single pixel and second the avoidance of searching for a correlation maximum in situations where there is no distinct peak in the correlation. Instead, it fully resolves the non-Gaussian velocity PDF.

REFERENCES

Raffel, M., Willert, C.E. Wereley, S.T., Kompenhans, J., 2007: “Particle Image Velocimetry: A Practical Guide”, Springer, Berlin, chapt. 5
Meinhart, C.D., Werely S.T., 2000: “A PIV algorithm for estimating time-averaged velocity fields”, Journal for Fluids Engineering, 122, pp. 285-289
Westerweel, J., Geelhoed, P.F., Lindken, R., 2004: “Single-pixel resolution ensemble correlation for micro-PIV applications”, Experiments in Fluids, vol. 37, pp. 375-384
Kähler, C.J., Scholz, U., Ortmanns, J., 2006: “Wall-shear-stress and near-wall turbulence measurements up to single pixel resolution by means of long-distance micro-PIV”, Experiments in Fluids, vol. 41, pp. 327-341
Scharnowski, S., Hain, R., Kähler, C.J., 2012: “Reynolds stress estimation up to single-pixel resolution using PIV-measurements”, Experiments in Fluids, vol. 52, pp. 985-1002
Moser, R.D., Kim, J., Mansour, N.N., 1999: “Direct numerical simulation of turbulent channel flow up to Re_τ=590”, Physics of Fluids, vol. 11, pp. 943-945